Received: 23 May 2023 | Revised: 23 September 2023 | Accepted: 29 September 2023

DOI: 10.1111/cts.13679

ARTICLE

Prediction of molecular phenotypes for novel *SCN1A* variants from a Turkish genetic epilepsy syndromes cohort and report of two new patients with recessive Dravet syndrome

Kerem Teralı[1] | **Ayberk Türkyılmaz**[2] | **Safiye Güneş Sağer**[3] | **Alper Han Çebi**[2]

[1]Department of Medical Biochemistry, Faculty of Medicine, Cyprus International University, Nicosia, Cyprus

[2]Department of Medical Genetics, Faculty of Medicine, Karadeniz Technical University, Trabzon, Turkey

[3]Department of Pediatric Neurology, Kartal Dr. Lütfi Kırdar City Hospital, İstanbul, Turkey

Correspondence
Kerem Teralı, Cyprus International University Faculty of Medicine, Haspolat, 99258 Nicosia, Cyprus.
Email: kterali@ciu.edu.tr

Abstract

Dravet syndrome and genetic epilepsy with febrile seizures plus (GEFS+) are both epilepsy syndromes that can be attributed to deleterious mutations occurring in *SCN1A*, the gene encoding the pore-forming α-subunit of the $Na_V1.1$ voltage-gated sodium channel predominantly expressed in the central nervous system. In this research endeavor, our goal is to expand our prior cohort of Turkish patients affected by *SCN1A*-positive genetic epilepsy disorders. This will be accomplished by incorporating two recently discovered and infrequent index cases who possess a novel biallelic (homozygous) *SCN1A* missense variant, namely E158G, associated with Dravet syndrome. Furthermore, our intention is to use computational techniques to predict the molecular phenotypes of each distinct *SCN1A* variant that has been detected to date within our center. The correlation between genotype and phenotype in Dravet syndrome/GEFS+ is intricate and necessitates meticulous clinical investigation as well as advanced scientific exploration. Broadened mechanistic and structural insights into $Na_V1.1$ dysfunction offer significant promise in facilitating the development of targeted and effective therapies, which will ultimately enhance clinical outcomes in the treatment of epilepsy.

Study Highlights

WHAT IS THE CURRENT KNOWLEDGE ON THE TOPIC?

Molecular phenotypes hold substantial potential for linking genetic variation to human disease. Numerous (mostly heterozygous) non-synonymous variants in *SCN1A* are able to result in epileptic phenotypes, such as Dravet syndrome and genetic epilepsy with febrile seizures plus (GEFS+), where the pathobiological basis may not be clear due to lack of mutant $Na_V1.1$ structures.

WHAT QUESTION DID THIS STUDY ADDRESS?

Here, we report a novel biallelic (homozygous) *SCN1A* missense variant, namely c.473A>G (p.Glu158Gly), in two siblings from consanguineous parents and

accordingly extend our previous Turkish genetic epilepsy syndromes cohort. Perhaps more interestingly, we show that the parents, who are heterozygous for the same variant, present with a milder GEFS+ phenotype. We also run computational experiments to gain further insights into $Na_V1.1$ dysfunction induced by the etiological mutations in our cohort.

WHAT DOES THIS STUDY ADD TO OUR KNOWLEDGE?

Our work provides additional evidence that homozygous variants in *SCN1A* can lead to Dravet syndrome. The range of clinical findings in the patients exhibiting autosomal recessive phenotypes associated with *SCN1A* is remarkably similar to that of other patients displaying autosomal dominant inheritance patterns, indicating a corresponding genotype–phenotype correlation.

HOW MIGHT THIS CHANGE CLINICAL PHARMACOLOGY OR TRANSLATIONAL SCIENCE?

In silico dissection of molecular phenotypes, including changes in protein stability and modifications to protein–protein interaction affinity, for non-synonymous variants in *SCN1A* will allow for a better understanding of the causal mechanisms underlying genetic epilepsy syndromes and facilitate the development of efficacious and targeted therapies to improve clinical outcomes in epilepsy.

INTRODUCTION

Voltage-gated sodium (Na_V) channels are crucial for action potential initiation and propagation in excitable cells. Human Na_V channels comprise a large pore-forming α-subunit and one or two smaller auxiliary β-subunits, resulting in nine isoforms ($Na_V1.1$ to $Na_V1.9$) based on α-subunit sequence.[1,2] The α-subunit is composed of 24 α-helical transmembrane segments distributed among four homologous repeats (R_I to R_{IV}), interconnected by intracellular loops. The S1–S4 segments in each repeat form the voltage-sensing domain (VSD), whereas the S5–S6 segments constitute the pore domain (PD). P1 and P2 helices connect the S5–S6 segments in each PD, enclosing the extracellular P-loop contributing to the selectivity filter (SF), known as the DEKA (Asp-Glu-Lys-Ala) locus, responsible for Na^+ ion selectivity.[3] Glycosylation sites on extracellular loops impact Na_V channel maturation and trafficking.[4] The S4 segment's positively charged residues, typically Arg, serve as gating charges (GCs), responding to membrane potential alterations. Movement of these GCs, catalyzed by sequential formation of ion pairs with negatively charged residues (usually Glu) in the S2 and S3 segments, induces conformational changes in the PD, referred to as electromechanical coupling.[5] This process involves activation, inactivation, and recovery, with a slow voltage-dependent and a fast millisecond-timescale inactivation mechanism in Na_V channels. The latter includes a fast-inactivation particle, termed the IFM (Ile-Phe-Met) motif, occluding the intracellular pore.[6]

Encoded by the *SCN1A* gene on chromosome 2 ($2q^{24.3}$), $Na_V1.1$ is among prominent sodium channels within the central nervous system (CNS) along with $Na_V1.2$, $Na_V1.3$, and $Na_V1.6$.[1,2] The recently solved three-dimensional structure of the full-length human $Na_V1.1$ α-subunit in complex with the auxiliary subunit β4[7] reveals that $Na_V1.1$ retains all the aforementioned hallmarks of Na_V channels (Figure 1). $Na_V1.1$ dysfunction, acquired or inherited, underlies various disorders, including Dravet syndrome and genetic epilepsy with febrile seizures plus (GEFS+). Dravet syndrome involves epileptic encephalopathy marked by febrile-triggered tonic–clonic seizures, often accompanied by cognitive deficits and ataxia.[8] GEFS+ is a familial epilepsy syndrome, with diverse seizure patterns and normal cognition.[9] $Na_V1.1$ channelopathies, besides trafficking and expression defects, result from altered gating properties, such as activation and inactivation.[10] Loss-of-function mutations generally cause reduced peak sodium current (I_{Na}), depolarizing shifts of the activation curve, hyperpolarizing shifts of the inactivation curve, and slower recovery from inactivation. Conversely, gain-of-function mutations usually cause late sodium current ($I_{Na,L}$), hyperpolarizing shifts of the activation curve, depolarizing shifts of the inactivation curve, and slower/disrupted inactivation. Some mutations induce opposing changes, complicating predictions of their impact on neuronal excitability.[10]

Until recently, Dravet syndrome's molecular mechanism was attributed solely to complete loss of function of $Na_V1.1$ in patients heterozygously affected, leading to inhibitory neuron haploinsufficiency in the CNS.[11,12] This theory was grounded in the interdependence of inhibitory and excitatory neurons in the CNS, whereby impaired $Na_V1.1$ function in inhibitory neurons decreases

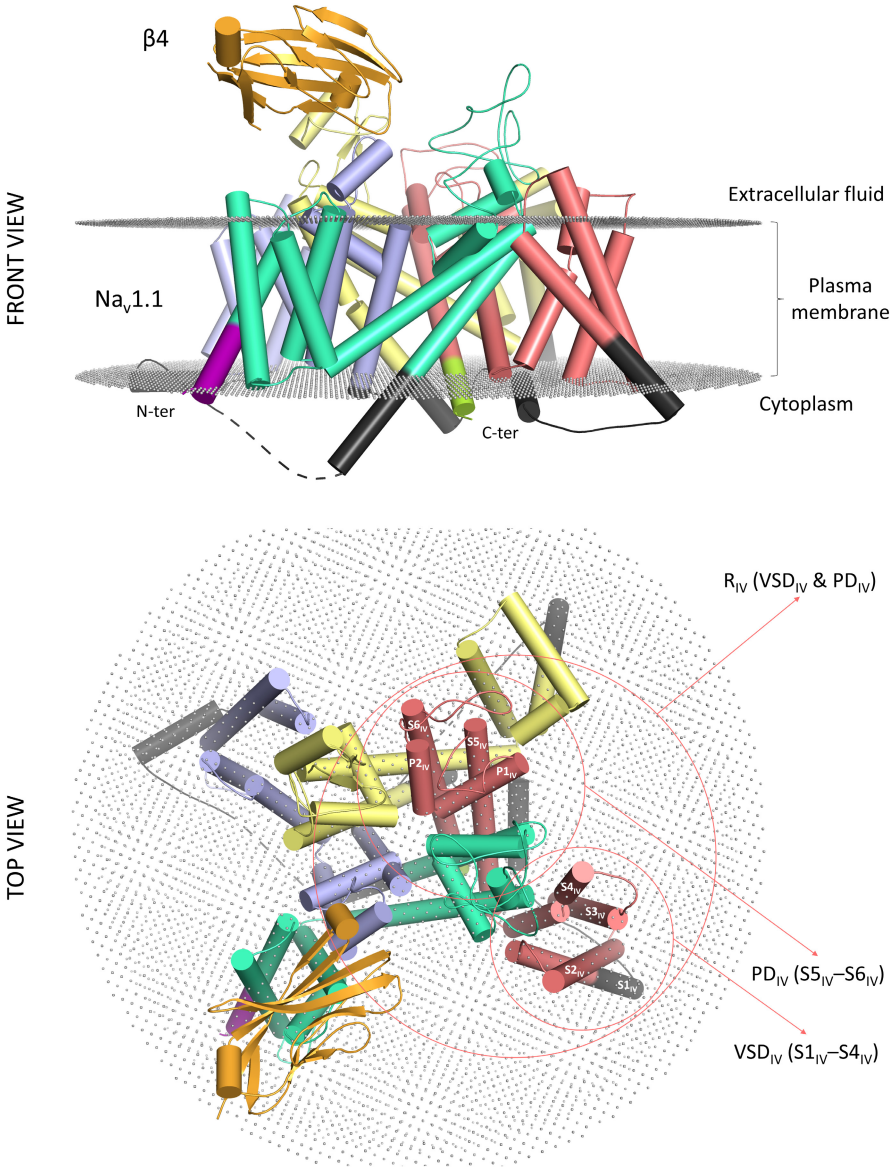

FIGURE 1 Cartoon representation of human $Na_V1.1$ complexed with β4 (PDB ID: 7DTD). The α-helices are shown as cylinders. R_I, R_{II}, R_{III}, and R_{IV} are colored aqua green, light blue, pale yellow, and salmon pink, respectively. Visible part of the $Na_V1.1$ NTD is colored purple, and visible part of the $Na_V1.1$ CTD is colored lime green. The cytoplasmic inter-repeat linkers are colored black. Dashed lines indicate the invisible regions of the channel. The images were rendered with the PyMOL Molecular Graphics System, v18 (Schrödinger LLC).

inhibition and raises excitatory activity, culminating in seizures. Recent research identified missense mutations in $Na_V1.1$ displaying gain-of-function gating properties, destabilizing inactivation particularly under elevated temperatures.[13,14] Fever-induced seizure onset in patients with Dravet syndrome underscores this observation. Some gain-of-function mutations exacerbate the phenotype compared to typical *SCN1A*-positive Dravet syndrome.[15,16] Contrarily, partial loss of function of $Na_V1.1$, potentially due to missense variants with detectable I_{Na}, aligns with milder GEFS+ phenotypes,[17,18] albeit sometimes intensified by seizures.[19] Similar to Dravet syndrome, certain GEFS+ *SCN1A* variants result in $Na_V1.1$ gain-of-function.[20,21] It is hypothesized that these missense mutations may hyperexcite excitatory neurons or trigger paradoxical γ-aminobutyric acid (GABA)ergic excitation. However, further investigations are needed. Overall, these findings underscore the need for deeper understanding of Dravet syndrome and GEFS+, emphasizing the significance of targeting enhanced $Na_V1.1$ activity.

Here, we aim at extending our previous Turkish cohort with Dravet syndrome and GEFS+ spectrum[22] through adding two new and uncommon index cases harboring a novel Dravet syndrome-associated biallelic (homozygous) *SCN1A* missense variant, as well as at computationally predicting molecular phenotypes for each novel *SCN1A* variant identified in our laboratory.

METHODS

Molecular genetic studies

This study was approved by the institutional ethics committee of Erzurum Training and Research Hospital (approval number: 2020/23-218). Written informed consents

were obtained from all parents in our outpatient clinics. Genomic DNA was isolated from the peripheral blood of patients with Dravet syndrome or GEFS+ using the QIAamp DNA Blood Mini QIAcube Kit (Qiagen) as per the manufacturer's protocols. The genomic DNA samples were subsequently genotyped by next-generation sequencing (NGS) using a *SCN1A*-gene-specific (sequence reference: NM_001165963, NP_001159435) commercial kit (Blueprint Genetics). The NGS process was performed on the Illumina MiSeq platform (Illumina). To establish the pathogenicity of any novel variants, in silico prediction tools (MutationTaster, SIFT, Provean, PolyPhen2, and CADD), population-based allele frequencies (1000G, gnomAD, and ExAC), ClinVar, and Human Gene Mutation Database, and American College of Medical Genetics and Genomics (ACMG) criteria were used.[23]

Computational biochemical studies

The cryo-electron microscopic structure of $Na_V1.1$ representing the inactivated state (PDB ID: 7DTD; resolution: 3.30 Å; aggregation state: particle; reconstruction method: single-particle)[7] was retrieved from the Orientations of Proteins in Membranes database for positioning of transmembrane proteins in lipid bilayers.[24] A homology model of the $Na_V1.1$ CTD was built based on the x-ray crystallographic structure of the $Na_V1.5$ CTD in complex with Mg^{2+}-bound CaM poised for activation (PDB ID: 4OVN; resolution: 2.80 Å; R_{free}: 0.282; R_{work}: 0.211)[25] using the SWISS-MODEL web server for protein structure prediction.[26] Besides $Na_V1.1$ and $Na_V1.5$ have homologous CTDs, the selected Ca^{2+}-free template is proposed to provide more useful insights into intermolecular interactions responsible for the physiological activation and pathophysiology of Na_V channels compared to the $Na_V1.5$ CTD–CaM–Ca^{2+} complexes whose structures were also elucidated at atomic resolution. CaM was extracted from the $Na_V1.5$ CTD crystal structure and merged with the $Na_V1.1$ CTD homology model. The resulting $Na_V1.1$ CTD–CaM complex was subjected to 100 steps of steepest descent energy minimization (step size: 0.02 Å) followed by 10 steps of conjugate gradient energy minimization (step size: 0.02 Å) using the Minimize Structure utility of UCSF Chimera.[27] Both the number and size of minimization steps indicated here correspond to the default values used for relieving any poor contacts that might arise between the two chains (steepest descent minimization) and reaching an energy minimum after the close contacts or clashes were relieved (conjugate gradient minimization). The atomistic structure of $Na_V1.1$ showing contacts between acyl tails and the channel as temperature factors (B-factors) was downloaded from the MemProtMD database for storing and analyzing the results of molecular dynamic simulations of transmembrane proteins in lecithin bilayer systems.[28] Mutant residues were introduced in silico using the Mutagenesis Wizard utility of the PyMOL Molecular Graphics System, version 1.8 (Schrödinger LLC), adopting the most common and least strained backbone-dependent rotamers. Amino acid sequences were aligned using the PSI/TM-Coffee web server for multiple sequence alignments of transmembrane proteins,[29] and sequence similarities and identities were rendered using the ESPript 3.0 program.[30]

RESULTS AND DISCUSSION

Genotypic and clinical phenotypic characteristics of the cohort

Mean age of onset of the first seizure was 20.4 ± 9 and 6.5 ± 2.5 months in the patients with the GEFS+ (5 cases) and Dravet syndrome (6 cases) phenotypes included in this study, respectively. The first seizure in all cases was febrile seizure. In all patients with Dravet syndrome, developmental delay, ataxia, and drug-resistant seizures were present. A total of eight different novel variants were detected in 11 index cases. Four of the nine individuals carrying a missense variant had the Dravet syndrome phenotype, and five had the GEFS+ phenotype. The Dravet syndrome phenotype was present in two individuals who had either a frameshift or a start-loss variant. In this report, clinical findings in patients from a family recently identified as having a novel biallelic *SCN1A* variant will be presented in depth. Clinical details of patients from other, independent families affected by *SCN1A*-positive GEFS+/Dravet syndrome can be found in our previous article.[22] A brief summary of the genotypic and phenotypic features of all cases are given in Table 1.

There were two siblings, who were compatible with the Dravet syndrome phenotype and were born from consanguineous parents, in the aforementioned family. Following NGS analysis of the DNA samples from the siblings (P1 and P2), we discovered a novel homozygous missense variant, namely c.473A>G (p.Glu158Gly), in the *SCN1A* gene. The parents (P3 and P4) were found to be heterozygous for the same variant. The variant was ultimately classified as likely pathogenic based on the ACMG guidelines.

P1 began having generalized clonic/myoclonic seizures when he was 4 months old. These generalized clonic and myoclonic seizures, with and without fever, lasted until he was 3 years old. The seizures were drug-resistant and occurred repeatedly with a frequency of ~20 times per day.

Vaccination provoked seizures. In addition, he presented with febrile status epilepticus. Seizures occurred exclusively during infection beyond the age of 3.5 years. The patient learned to walk when he was 2.5 years old. Currently, he suffers from ataxia and intention tremor. He appears to follow simple (2- to 3-word) commands. He shows severe global developmental delay.

P2 began having myoclonic seizures in the distal extremities around the mouth and eyes at the age of 2 months. She had febrile and afebrile generalized clonic seizures that were drug resistant once she was 12 months old. She had only infection-triggered seizures after the age of 3 years. Currently, she walks with assistance and suffers from ataxia and intention tremor. The patient makes eye contact but does not speak any meaningful words. She is also unable to follow directions. She shows severe global developmental delay.

Seizures in the mother (P3) started at the age of 12 months as febrile seizures, followed by generalized clonic seizures with and without fever that occurred about four or five times per month. There exists a history of febrile status epilepticus. Seizures occurred exclusively with infection after the age of 3 years, and they stopped at the age of 7 years.

Seizures in the father (P4) started at the age of 1 year, with the first febrile seizure followed by febrile and non-febrile seizures. He experienced only infection-triggered seizures after the age of 5 years. His last seizure occurred when he was 7 years old. The father began walking at the age of 2 years and talking at the age of 3 years.

The p.Arg1886Gly, p.Tyr1926Cys, and p.Arg1933Gln variants are localized in the $Na_V1.1$ CTD which interacts with diverse binding partners

The proximal $Na_V1.1$ CTD harbors an IQ motif (residues 1912–1938, with the highly conserved Ile-1922 and Gln-1923 residues residing in the middle of the motif) that is known to bind calmodulin (CaM), a prototypical and versatile Ca^{2+}-sensing protein. Ca^{2+}-free CaM (apoCaM or Mg^{2+}-bound CaM) pre-associates with the IQ motif through its C-lobe and is subject to an allosterically induced conformational change upon calcium binding, thereby regulating the gating properties and kinetics of Na_V channels.[31] In an attempt to predict the structural-functional roles of the variants p.Arg1886Gly, p.Tyr1926Cys, and p.Arg1933Gln in a channelopathic context, we homology-modeled the $Na_V1.1$ CTD in complex with Mg^{2+}-bound CaM.

Arg-1886 appeared to lie in a globular EF-hand-like (EFL) domain folded into an acidic five-helix (αI–αV) bundle, forming a salt bridge with a highly conserved glutamate residue, Glu-1890, from the same α-helix and hydrophobic interactions with a highly conserved phenylalanine residue, Phe-1869, from the opposite α-helix (Figure 2). Therefore, the substitution of a glycine residue for this arginine residue is expected to destabilize the EFL fold in $Na_V1.1$. This is corroborated by the estimates of the mCSM-membrane algorithm[32] which predicts the p.Arg1886Gly variant to exert a destabilizing effect on $Na_V1.1$, with a $\Delta\Delta G$ value of $-0.195\,kcal\,mol^{-1}$ (Table 1). The occurrence of a basic residue (Arg/Lys) at the corresponding position in other eight human Na_V channels attest to the significance of this positive charge for the CTD structure and/or function (Figure 2). In this regard, the p.Arg1886Gln variant has been associated with generalized tonic–clonic seizures and atypical absences in a pediatric patient with Dravet syndrome before.[33] The EFL domain of various Na_V isoforms has been shown to be important for binding to the cytoplasmic R_{III}–R_{IV} linker bearing the fast-inactivation gate IFM motif at particular times during the electromechanical coupling cycle of the channel[34,35] as well as to cytoplasmic fibroblast growth factor (FGF) homologous factors belonging to the non-secreted FGF family of growth factors,[36,37] thereby modulating channel inactivation. It is worth mentioning that P5 displays only anti-epileptic-drug-sensitive seizures compatible with GEFS+. Given the presence of a milder GEFS+ phenotype in this patient, the mutant Gly-1886 residue with its minimal side chain appears to disturb the structure of the $Na_V1.1$ CTD only partially.

Both Tyr-1926 and Arg-1933 lie in a long basic α-helix (αVI) that follows the EFL domain and contains the IQ motif with high affinity for CaM. The CaM modulates Na_V-mediated excitable activity in response to oscillations in intracellular Ca^{2+} concentration. Considered individually, Tyr-1926 seemed to insert its electron-rich side chain into a methionine cleft formed by Met-125 and Met-146 on the C-lobe of Ca^{2+}-depleted CaM, establishing sulfur–π interactions with these sulfur-bearing residues (Figure 2). The replacement of this tyrosine residue by a cysteine residue is likely to disrupt this protein–protein interaction network. Due to its cytoplasmic localization, the mutated cysteine residue probably does not participate in disulfide bond formation. The occurrence of an aromatic residue (other than tryptophan with its bulky side chain) at the corresponding position in $Na_V1.2$–$Na_V1.9$ reflects the key role played by these sulfur–π interactions in governing molecular recognition and complexation events during CaM binding to the Na_V CTD (Figure 2). These findings are likely to correlate to the manifestation of a more severe Dravet syndrome phenotype in P6 who has moderate intellectual disability, drug-resistant seizures, and ataxia.

TABLE 1 Variants found in patients with Dravet syndrome/GEFS+, in silico assessment of the variants' pathogenicity, and neuroclinical findings in the patients.

Patient ID	Genotype (NM_001165963)	Pred-MutHTP	mCSM-membrane: Pathogenicity	mCSM-membrane: Stability	Age of seizure onset & first seizure type
P1	c.473A>G (p.Glu158Gly) Hom	Disease-causing (confidence score: 0.996)	Pathogenic	Destabilizing ($\Delta\Delta G = -0.848$ kcal mol^{-1})	4 months Generalized clonic/ myoclonic seizures
P2	c.473A>G (p.Glu158Gly) Hom	Disease-causing (confidence score: 0.996)	Pathogenic	Destabilizing ($\Delta\Delta G = -0.848$ kcal mol^{-1})	2 months Generalized clonic/ myoclonic seizures
P3	c.473A>G (p.Glu158Gly) Het	Disease-causing (confidence score: 0.996)	Pathogenic	Destabilizing ($\Delta\Delta G = -0.848$ kcal mol^{-1})	12 months FS
P4	c.473A>G (p.Glu158Gly) Het	Disease-causing (confidence score: 0.996)	Pathogenic	Destabilizing ($\Delta\Delta G = -0.848$ kcal mol^{-1})	12 months FS
P5	c.5656C>G (p.Arg1886Gly) Het	Disease-causing (confidence score: 0.73)	Pathogenic	Destabilizing ($\Delta\Delta G = -0.195$ kcal mol^{-1})	2.5 years FS
P6	c.5777A>G (p.Tyr1926Cys) Het	Disease-causing (confidence score: 0.88)	Pathogenic	Destabilizing ($\Delta\Delta G = -0.27$ kcal mol^{-1})	9 months FS
P7	c.5798G>A (p.Arg1933Gln) Het	Disease-causing (confidence score: 0.592)	Pathogenic	Destabilizing ($\Delta\Delta G = -0.252$ kcal mol^{-1})	2.5 years FS
P8	c.2T>G (p.M1?) Het	–	–	–	9 months FS
P9	c.440T>C (p.Met147Thr) Het	Disease-causing (confidence score: 0.549)	Pathogenic	Destabilizing ($\Delta\Delta G = -0.624$ kcal mol^{-1})	1.5 years FS
P10	c.2332A>C (p.Ile778Leu) Het	Disease-causing (confidence score: 1)	Pathogenic	Stabilizing ($\Delta\Delta G = +0.129$ kcal mol^{-1})	4 months FS
P11	c.4167_4175delCGT GAATAAinsTG (p.Asn1391Ilefs*5) Het	–	–	–	3 months FS

Note: The 11 patients shown here harbor a novel variant, for which computational predictive approaches were implemented, and thus represent a selected subgroup of the entire cohort. P1–P4 were first described in the present study; P5–P11 were first described in.[22]

Abbreviations: –, absence; +, presence; CLB, clobazam; DS, Dravet syndrome; FS, febrile seizure; GEFS+, genetic epilepsy with febrile seizures plus; Het, heterozygous; Hom, homozygous; ID, intellectual disability; LEV, levetiracetam; PB, phenobarbital; VPA, valproic acid; $\Delta\Delta G$, difference in Gibbs free energy of folding.

Similarly, Arg-1933 extends its positively charged side chain from the same helix as Tyr-1926 directly toward a negatively charged patch on the C-lobe of CaM, being engaged in electrostatic interactions with Glu-124 and Glu-128 (Figure 2). The mutation of this arginine residue into a glutamine residue will cause loss of these electrostatic interactions which appear to provide an anchoring mechanism for the orientation of CaM binding to the $Na_V1.1$ CTD. Interestingly, an Arg-to-Gln change at the equivalent position can be tolerated in other Na_V isoforms, but only when the preceding amino acid is a basic one (Figure 2). This could be attributed to the excellent hydrogen-bonding capacity of the amide group of Gln, which partly compensates for the loss of Arg. Although a missense mutation at position 1933 in $Na_V1.1$ has not previously been reported in the relevant scientific literature,

Ataxia	Intellectual disability	Developmental or language delay	Drug-resistant seizures	Therapy and prognosis	Clinical phenotype
++	Too young for evaluation	+	+	Seizures are controlled with VPA, LEV, and CLB Still having infection-triggered seizures	DS
++	Too young for evaluation	+	+	Seizures are controlled with VPA, LEV, and CLB Still having infection-triggered seizures	DS
–	–	–	–	Seizures are controlled with single anti-seizure medication regimens	GEFS+
–	–	–	–	Seizures are controlled with single anti-seizure medication regimens	GEFS+
–	–	–	–	Seizures are controlled with PB	GEFS+
+	Moderate ID	+	+	Seizures are controlled with VPA Still having infection-triggered seizures	DS
–	–	–	–	Seizures are controlled with VPA	GEFS+
+	Too young for evaluation	+	+	Seizures are controlled with VPA, LEV, and CLB Still having infection-triggered seizures	DS
–	–	–	–	Seizures are controlled with VPA	GEFS+
++	Severe ID	+	++	Seizures are not well-controlled despite multidrug treatment regimens	DS
++	Severe ID	+	+	Seizures are controlled with VPA, LEV, and CLB Still having infection-triggered seizures	DS

an Arg-to-His substitution at the corresponding position in the cardiac-specific $Na_V1.5$ isoform (p.Arg1919His) has been demonstrated to lead to loss of function of $Na_V1.5$ (i.e., reduced peak I_{Na} density) using electrophysiological studies in a Japanese Brugada syndrome cohort.[38] However, it is worth emphasizing here that isoform-specific differences may exist not only with respect to CaM's regulatory role in channel function, but also with respect to the mode of CaM binding to the channel. For instance, Ca^{2+}/calmodulin-dependent protein kinase II (CaMKII)-mediated phosphorylation of the $Na_V1.1$ IQ domain has been found to increase the affinity of Ca^{2+}-loaded CaM for the channel.[39] Arg-1933 is located in the immediate vicinity of one of the three potential phosphorylation sites, namely Thr-1934. Therefore, replacement of Arg-1933 by another residue holds the possibility of

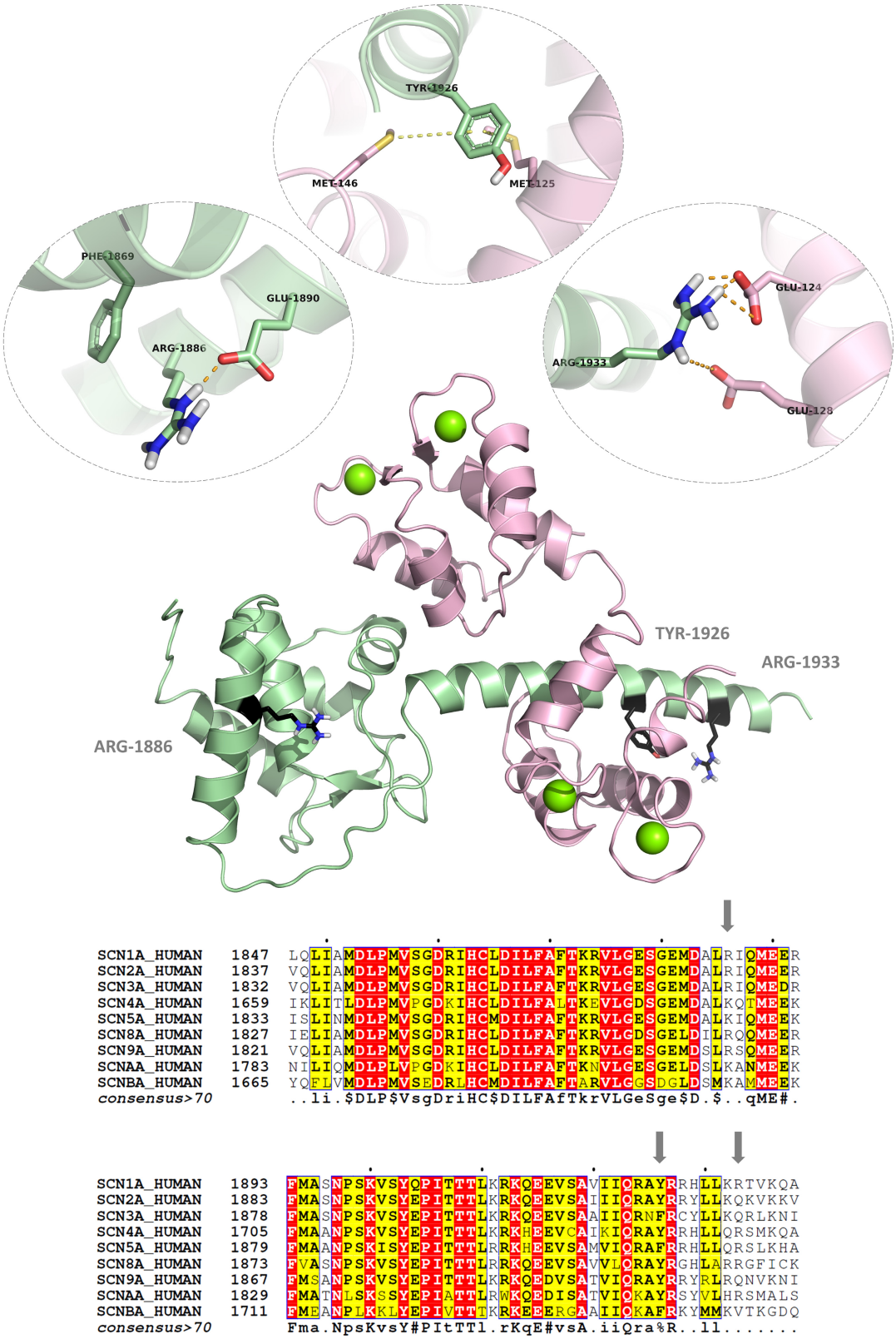

FIGURE 2 The $Na_V1.1$ CTD homology model (pale green) complexed with Mg^{2+}-bound CaM (light pink). The four Mg^{2+} ions are shown as lime green spheres. The side chains of the three affected amino acid residues are shown as black sticks. Top insets show the network of favorable non-covalent interactions around each affected residue. Electrostatic interactions are indicated by orange dashed lines, and sulfur–π interactions are indicated by yellow dashed lines. Bottom panels show parts of the multiple sequence alignment of all nine Na_V isoforms, with the position of each affected residue being marked by an arrow. The images were rendered with the PyMOL Molecular Graphics System, v18 (Schrödinger LLC). The graphically enhanced alignment was prepared with ESPript 3.0.

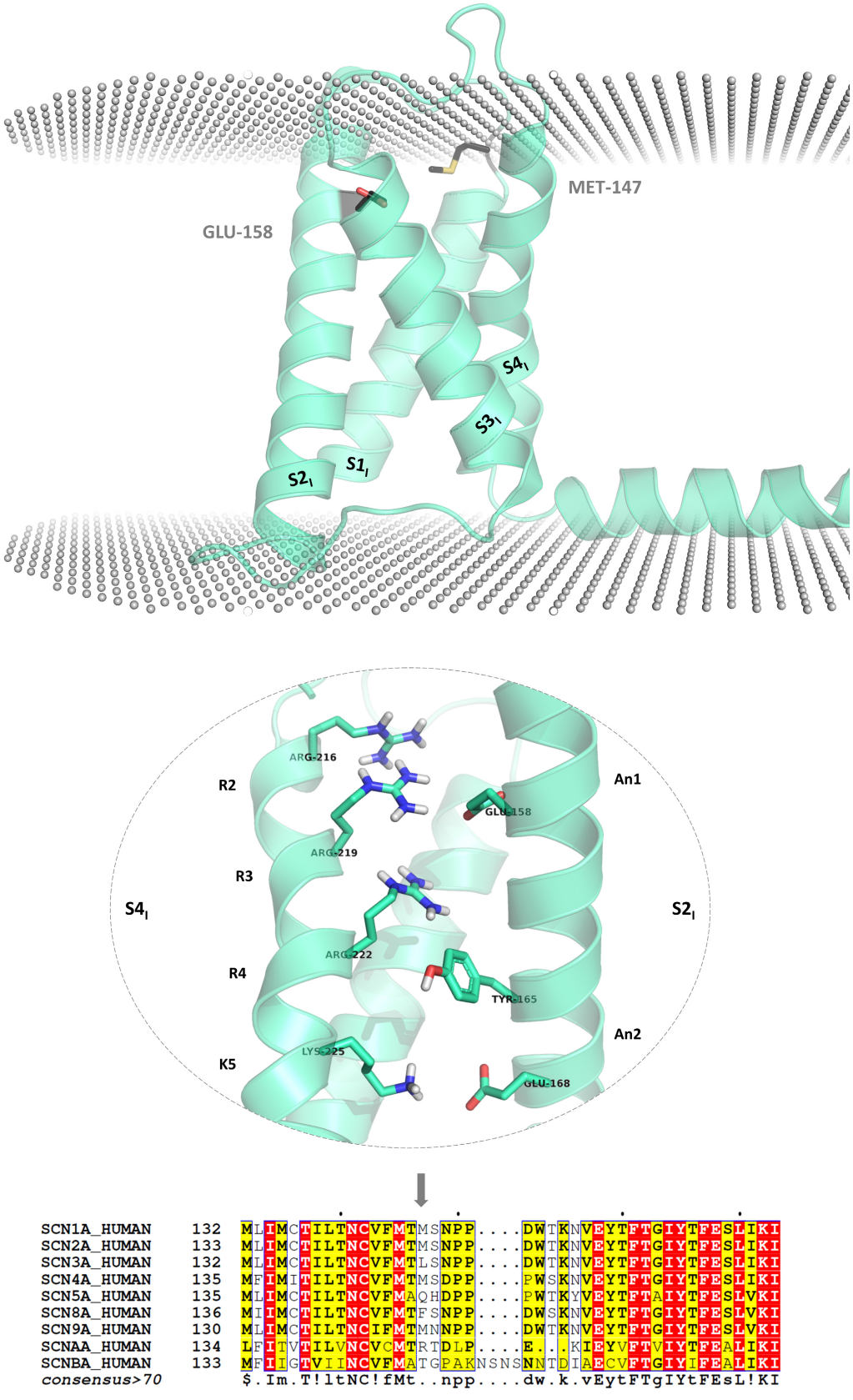

FIGURE 3 The $Na_V1.1$ VSD_I. The side chains of the two affected amino acid residues are shown as black sticks. Middle inset shows the orientation of Glu-158 relative to the basic GC residues of the gating pore. Bottom panel shows a part of the multiple sequence alignment of all nine Na_V isoforms, with the position of Met-147 marked by an arrow. The images were rendered with the PyMOL Molecular Graphics System, v18 (Schrödinger LLC). The graphically enhanced alignment was prepared with ESPript 3.0. GC, gating charge.

loosening the phosphorylation-induced binding of the N-lobe of Ca^{2+}/CaM to the $Na_V1.1$ CTD through altering the substrate recognition motif of CaMKII. Overall, our in silico data suggest partial loss of function of the channel, compatible with GEFS+. This is possibly corroborated by the sole finding of anti-epileptic-drug-sensitive seizures in P7.

The curious cases of the p.Met1Arg and p.Met147Thr variants

The p.Met1Arg variant, or more truly perhaps the M1? mutation, replaces the initial methionine residue of $Na_V1.1$ and may, in a worst-case scenario, result in a complete lack of the full-length protein through interfering with the translation process. The next in-frame Met residue occurs at position 72, but experimental studies demonstrating the potential use of this downstream Met residue are missing. The use of Met-72 as an alternative translation initiation site will remove slightly more than the first half (~55%) of the amino acids from the $Na_V1.1$ NTD, yielding a truncated protein. To date, no functional role for the $Na_V1.1$ NTD has been described. Contrarily, the $Na_V1.2$ NTD has been shown to contribute to the axonal localization in neurons and apical localization in Madin–Darby canine kidney cells, a common model system for studies of membrane protein sorting, of this particular isoform.[40] Similarly, the $Na_V1.6$ NTD has been found to be required for channel trafficking between the Golgi apparatus and the plasma membrane.[41] A recent study has even suggested that the $Na_V1.5$ NTD serves as a binding site for CaM, a well-established Na_V CTD partner protein.[42] Collectively, our findings indicate that the M1? mutation is most likely deleterious and leads to loss of function of $Na_V1.1$, possibly explaining the occurrence of Dravet syndrome in P8 who displays developmental delay, drug-resistant seizures, and ataxia.

Met-147 sits in the beginning of the $S1_I$–$S2_I$ linker (residues 147–152) and is positioned to make hydrophobic contacts with neighboring residues moderately to highly conserved among different human Na_V channel isoforms, including Phe-144 and Pro-150 (Figure 3). There exist major physicochemical differences between Met and Thr, and a Met-to-Thr substitution at position 147 is expected to weaken the local hydrophobic interactions mentioned already. This may pose a potential folding/stability problem, as estimated from the difference in Gibbs free energy of folding (Table 1). It was interesting to note that both the corresponding residue and the succeeding residue (Ser-148 in $Na_V1.1$) were not conserved evolutionarily in other eight human Na_V channels (Figure 3). This, however, was not the case with a selected sample of mammalian (mouse, rat, rabbit, bovine, pig, chimpanzee, and goat) $Na_V1.1$ channels in which this Met residue was found to be strictly conserved (data not shown). The latter observation suggests that Met-147 is likely to play an isoform-specific role in channel activity. Intriguingly, it has been documented that the S1–S2 linker contributes to the creation of gating-modifier toxin recognition sites on different Na_V VSDs.[43–46] It could be that Met-147 is involved in directly interacting with a yet-to-be-identified peptide ligand (which could be either exogenous or endogenous in origin) modulating $Na_V1.1$ gating or that Met-147 is required for the correct folding and/or conformational stability of the $S1_I$–$S2_I$ loop mediating $Na_V1.1$–ligand interactions. The diagnosis of GEFS+ manifested by anti-epileptic-drug-sensitive seizures in P9 plausibly implies the adverse but relatively minor impact of the p.Met147Thr variant on $Na_V1.1$ function.

The p.Glu158Gly variant affects one of the several GC-coordinating residues of the $Na_V1.1$ VSD_I

The $S4_I$ segment of $Na_V1.1$ carries four GC residues involving Arg-216 (designated R2), Arg-219 (designated R3), Arg-222 (designated R4), and Lys-225 (designated K5). In response to membrane depolarization, these GCs are believed to form sequential ion pairs with anionic centers (designated An1 and An2) that are represented by two glutamate side chains spaced 10 residues apart on the $S2_I$ segment.[5] An1 and An2 are separated by Tyr-165, also known as the hydrophobic constriction site (HCS), which prevents ion leakage by enforcing a bottleneck effect around the gating pore. Through facilitating the upward movement of GCs, both An1 and An2, together with an invariant aspartate residue on the $S3_I$ segment, allow for channel activation and pore opening. The majority of solved structures of drug-, toxin-, or mutation-free human Na_V channels, including the $Na_V1.1$ structure exploited in the present study, share a similar conformation characterized by an almost closed pore and partially "up" GCs, consistent with the inactivated state.

Glu-158, which corresponds to An1, appeared to coordinate R3 in the inactivated state of the channel (Figure 3). A Glu-to-Gly change at position 158 will lead to loss of this negative charge center with possible implications for channel dysfunction. Intriguingly, the p.Glu158Gly variant that was reported for the first time in this study was observed to be inherited in an autosomal recessive manner from consanguineous parents with heterozygous genotypes. Biallelic mutations in *SCN1A* are thought of as a rare genetic subtype in patients with Dravet syndrome/GEFS+.[47] In a previous study, the presence of $Na_V1.1$

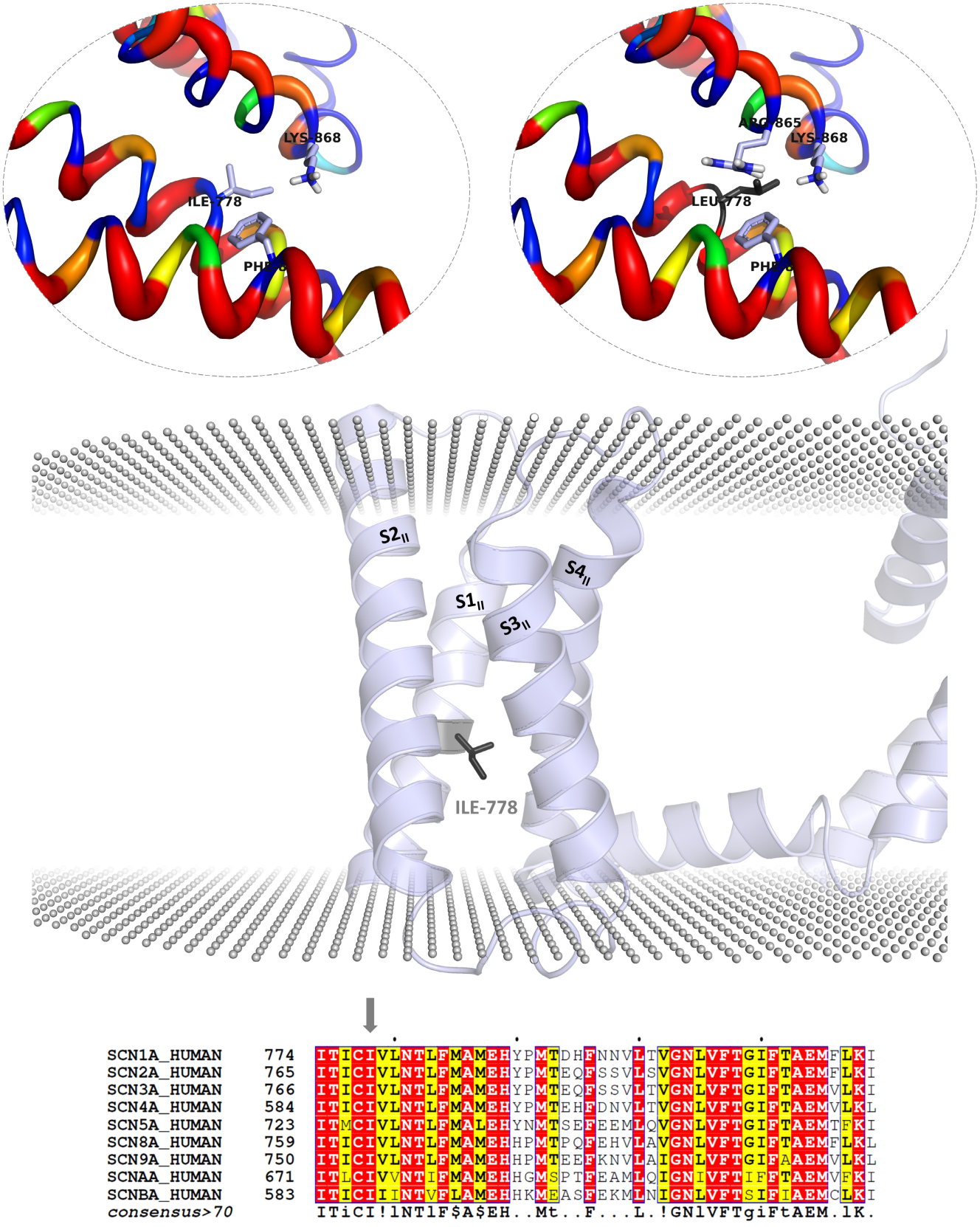

FIGURE 4 The $Na_V1.1$ VSD_{II}. The side chain of the affected amino acid residue is shown as black sticks. Top left inset shows the neighboring residues involved in hydrophobic contacts with the wild-type residue, and top right inset shows the neighboring residues involved in hydrophobic contacts with the mutant residue. Bottom panel shows a part of the multiple sequence alignment of all nine Na_V isoforms, with the position of Ile-778 marked by an arrow. The images were rendered with the PyMOL Molecular Graphics System, v18 (Schrödinger LLC). The graphically enhanced alignment was prepared with ESPript 3.0.

p.Glu158Gln, which was categorized as pathogenic/likely pathogenic by the researchers of the study, in a heterozygous state was shown to be associated with disease in an unselected cohort of ~8.6 thousand patients with epilepsy and neurodevelopmental disorders.[48] Furthermore, the replacement of the corresponding glutamate residue in $Na_V1.5$ by either a glutamine[49] or a lysine[50] residue was reported to be possibly causative for Brugada syndrome, a clinical phenotype typically arising from loss-of-function defects. The $Na_V1.5$ p.Glu161Lys variant was later shown to result in reduced peak I_{Na} and a depolarizing shift in the activation curve in the tsA201 human embryonic kidney cells transfected with both the mutant $Na_V1.5$ α-subunit and the wild-type β1-subunit.[51] These findings suggest that not only charge-reversal mutations but also charged-to-polar mutations at this position provide a pathogenic substrate for disease. Glycine, on the other hand, is neither positively charged nor polar, and this warrants additional studies of the electrophysiological type so as to explore the precise role of the mutant Gly-158 residue in $Na_V1.1$ gating. Substitution of VSD residues, especially the GC residues and those that facilitate the voltage-dependent motion of GC residues, mainly bring about shifts of the activation and/or inactivation curve(s).[7] It could be that the p.Glu158Gly variant is accompanied by a partial deficit in $Na_V1.1$ gating or that the discrete activating and inactivating effects of p.Glu158Gly on the gating properties of $Na_V1.1$ somewhat neutralize each other, producing a hypomorphic allele. This is partially in agreement with the observation that the affected siblings' parents (P3 and P4), who are heterozygous for the p.Glu158Gly variant, present with a milder GEFS+ phenotype. We do not, however, exclude the possibility that any further dysfunctional variant is present in a gene not yet linked to epilepsy, or in a regulatory intronic region of *SCN1A*. It is also worth noting here that, in addition to genetic factors, epigenetic and environmental influences may also be responsible for shaping the epileptic phenotype.

The significance of the p.Ile778Leu variant is derived from its atomic proximity to the GCs of the $Na_V1.1$ VSD_{II} in the inactivated state of the channel

Virtually, the p.Ile778Leu variant represents a very conservative mutation that affects the $S1_{II}$ segment of $Na_V1.1$ (Figure 4). Molecular dynamic simulations showing the average occupancy of the fatty acyl chains of lecithin molecules within 6 Å of the channel on an 800-ns timescale revealed that Ile-778 did not form contacts with the lipid tails (Figure 4). In the current (possibly inactivated) state of the channel, Ile-778 seemed to establish hydrophobic contacts with the GC residue Lys-868 (K5) on the $S4_{II}$ segment and the HCS residue Phe-811 on the $S2_{II}$ segment. In silico introduction of the Leu-778 residue caused minor steric clashes, or van der Waals overlaps, with Lys-868, Phe-811, and an additional GC residue, Arg-865 (R4), in the $Na_V1.1$ VSD_{II}. Although no further attempt was made to refine the mutant $Na_V1.1$ structure, it is plausible to assume that Leu-778 can readily be accommodated in the same region as Ile-778. Being isomers of each other, Ile and Leu have similar shapes and electronic properties but different symmetries and exposed surface areas. The Leu-778 side chain was more protruding compared to the β-branched Ile-778 side chain and favored increased hydrophobic contacts with the surrounding GC residues on the $S4_{II}$ segment (Figure 4). It could be that the difference in the side-chain characteristics yielded a distinct local interaction network, possibly maximizing helix–helix contacts in the $Na_V1.1$ VSD_{II}. This is in accordance with the finding that the p.Ile778Leu variant was predicted to have a stabilizing effect on $Na_V1.1$, with a $\Delta\Delta G$ value of $+0.129\,kcal\,mol^{-1}$ (Table 1). In most simple terms, stabilization of the present conformational state of $Na_V1.1$ is expected to promote inactivation, that is, to result in a left shift of the inactivation curve. However, given its critical localization within the channel, Ile-778 is likely to play an additional, specific role in $Na_V1.1$ gating. Ile-778 sits at the protein–solvent interface of the $Na_V1.1$ VSD_{II} and is within atomic proximity of the $S4_{II}$ segment at the level of K5. The p.Ile778Leu variant may thus affect (e.g., slow or arrest) the movement of the $Na_V1.1$ VSD_{II}. The results of our multiple sequence alignment also highlighted the invariant nature of this Ile residue among the nine human Na_V isoforms examined in this study (Figure 4). Although our computational predictions provide positive evidence of the mutation's severity and therefore seemingly correlate to the development of Dravet syndrome in P10 (which is manifested by severe intellectual disability, drug-resistant seizures, and ataxia), the field awaits electrophysiological support for the mechanistic insights proposed herein.

The p.Asn1391Ilefs*5 variant is a frameshift one that truncates the channel shortly before the SF zone of the $Na_V1.1$ PD_{III}

Asn-1391 lies in the extracellular loop that bridges the $S5_{III}$ segment with the $P1_{III}$ helix and is right next to an *N*-glycosylation site (Asn-1392). It has been proposed that missense variants mapped to the $Na_V1.1$ VSDs and to the channel's segments implicated in pore gating and fast inactivation represent function-disturbing mutations, whereas those mapped to the extracellular loops above the $Na_V1.1$ PD and to the P1-SF-P2 region (designated the

SF zone) of the channel represent structure-disturbing mutations.[7] The former alter electrophysiological properties of the channel, such as conductance and activation/inactivation kinetics, whereas the latter impact channel folding, trafficking, and interactions with various binding partners. Although hundreds of missense variants related to genetic epilepsy syndromes with varying degrees of severity have been identified to date, more than half of epileptogenic mutations in *SCN1A* are truncating variants.[7] The frameshift variant p.Asn1391Ilefs*5 introduces a premature termination codon (PTC) five amino acids downstream of the affected Asn residue, truncating $Na_V1.1$ in the extracellular portion of its PD_{III}. This most probably leads to haploinsufficiency either via degradation of the PTC-containing transcript by the action of the nonsense-mediated mRNA decay system or via altered processing and rapid clearance of the truncated polypeptide. The resulting loss-of-function allele is, in part, consistent with the dominant Dravet syndrome phenotype observed in P11 who has severe intellectual disability, drug-resistant seizures, and ataxia. One nonsense variant, p.Cys1396*, mapped to the same extracellular loop of the $Na_V1.1$ PD_{III}, for example, was shown to be associated with Dravet syndrome in a cohort of *SCN1A*-positive Chinese patients.[52] Two other nonsense variants, p.Arg1407* and p.Trp1408*, located slightly further downstream from Asn-1391 were also demonstrated to be related to Dravet syndrome in Hungarian[53] and Japanese[54] populations, respectively. These previous reports provide additional support for the overall assumption we made.

CONCLUSION

By leveraging in silico methods, such as molecular modeling, simulation, and data analysis, computational biology enables a comprehensive understanding of the functional consequences of newly discovered disease-associated variants. This is particularly crucial for rare diseases, where traditional genetic screening methods often fall short due to limited sample sizes and genetic heterogeneity. Nevertheless, this approach is not without its limitations. As whole-exome or -genome sequencing becomes more widely applied, the sheer volume of identified rare variants is set to surge, posing significant challenges in discerning true causative mutations from benign ones. Furthermore, functional validation of identified variants remains a formidable task, often requiring laborious and resource-intensive experimental work. Our study contributes supplementary substantiation to the notion that homozygous variants within the *SCN1A* gene are likely to precipitate the onset of Dravet syndrome. The spectrum of clinical observations observed in individuals manifesting autosomal recessive phenotypic expressions tied to *SCN1A* closely parallels the presentation observed in other cases demonstrating an autosomal dominant inheritance pattern, thereby implying a concordant relationship between mutant genotype and clinical phenotype. Additionally, our work stresses the importance of predicting molecular phenotypes, such as changes in protein stability and modifications to protein–protein interaction affinity, for each newly discovered non-synonymous *SCN1A* variant, which considerably helps to unravel the structural and mechanistic basis of potential $Na_V1.1$ dysfunction in genetic epilepsy syndromes. These calculations, however, do not replace the necessary electrophysiological studies in cell cultures and/or animal models, which are beyond the scope of this report. Currently, they are the ultimate method of choice to establish that $Na_V1.1$ channel dysfunction occurs and is the causal link between epilepsy and an *SCN1A* variant.

AUTHOR CONTRIBUTIONS

K.T. and A.T. wrote the manuscript. K.T. and A.T. designed the research. K.T., A.T., S.G.S., and A.H.Ç. performed the research. K.T., A.T., and A.H.Ç. analyzed the data.

FUNDING INFORMATION

Kerem Terali was supported by the Uluslararasi Kibris Universitesi. Within the scope of the EKUAL project carried out by TUBITAK ULAKBIM, Cyprus International University will pay the article processing charge.

CONFLICT OF INTEREST STATEMENT

The authors declared no competing interests for this work.

DATA AVAILABILITY STATEMENT

The data that support the findings of this study are available upon reasonable request from the authors.

ORCID

Kerem Terali https://orcid.org/0000-0002-9964-6383

REFERENCES

1. Catterall WA. Voltage-gated sodium channels at 60: structure, function and pathophysiology. *J Physiol*. 2012;590:2577-2589.
2. Goldin AL. Resurgence of sodium channel research. *Annu Rev Physiol*. 2001;63:871-894.
3. Favre I, Moczydlowski E, Schild L. On the structural basis for ionic selectivity among Na^+, K^+, and Ca^{2+} in the voltage-gated sodium channel. *Biophys J*. 1996;71:3110-3125.
4. Schmidt JW, Catterall WA. Biosynthesis and processing of the α subunit of the voltage-sensitive sodium channel in rat brain neurons. *Cell*. 1986;46:437-445.
5. Catterall WA. Ion channel voltage sensors: structure, function, and pathophysiology. *Neuron*. 2010;67:915-928.

6. Catterall WA, Wisedchaisri G, Zheng N. The chemical basis for electrical signaling. *Nat Chem Biol*. 2017;13:455-463.
7. Pan X, Li Z, Jin X, et al. Comparative structural analysis of human $Na_v1.1$ and $Na_v1.5$ reveals mutational hotspots for sodium channelopathies. *Proc Natl Acad Sci*. 2021;118:e2100066118.
8. Scheffer IE, Nabbout R. *SCN1A*-related phenotypes: epilepsy and beyond. *Epilepsia*. 2019;60:S17-S24.
9. Zhang YH, Burgess R, Malone JP, et al. Genetic epilepsy with febrile seizures plus: refining the spectrum. *Neurology*. 2017;89:1210-1219.
10. Fouda MA, Ghovanloo MR, Ruben PC. Late sodium current: incomplete inactivation triggers seizures, myotonias, arrhythmias, and pain syndromes. *J Physiol*. 2022;600:2835-2851.
11. Dravet C. The core Dravet syndrome phenotype. *Epilepsia*. 2011;52:3-9.
12. Rubinstein M, Han S, Tai C, et al. Dissecting the phenotypes of Dravet syndrome by gene deletion. *Brain*. 2015;138:2219-2233.
13. Peters C, Rosch RE, Hughes E, Ruben PC. Temperature-dependent changes in neuronal dynamics in a patient with an *SCN1A* mutation and hyperthermia induced seizures. *Sci Rep*. 2016;6:31879.
14. Gorman KM, Peters CH, Lynch B, et al. Persistent sodium currents in *SCN1A* developmental and degenerative epileptic dyskinetic encephalopathy. *Brain Commun*. 2021;3:fcab235.
15. Berecki G, Bryson A, Terhag J, et al. *SCN1A* gain of function in early infantile encephalopathy. *Ann Neurol*. 2019;85:514-525.
16. Clatot J, Parthasarathy S, Cohen S, et al. *SCN1A* gain-of-function mutation causing an early onset epileptic encephalopathy. *Epilepsia*. 2023;64:1318-1330.
17. Mantegazza M, Gambardella A, Rusconi R, et al. Identification of an $Na_v1.1$ sodium channel (SCN1A) loss-of-function mutation associated with familial simple febrile seizures. *Proc Natl Acad Sci*. 2005;102:18177-18182.
18. Kluckova D, Kolnikova M, Lacinova L, et al. A study among the genotype, functional alternations, and phenotype of 9 *SCN1A* mutations in epilepsy patients. *Sci Rep*. 2020;10:10288.
19. Salgueiro-Pereira AR, Duprat F, Pousinha PA, et al. A two-hit story: seizures and genetic mutation interaction sets phenotype severity in SCN1A epilepsies. *Neurobiol Dis*. 2019;125:31-44.
20. Lossin C, Rhodes TH, Desai RR, et al. Epilepsy-associated dysfunction in the voltage-gated neuronal sodium channel SCN1A. *J Neurosci*. 2003;23:11289-11295.
21. Spampanato J, Kearney JA, De Haan G, et al. A novel epilepsy mutation in the sodium channel SCN1A identifies a cytoplasmic domain for β subunit interaction. *J Neurosci*. 2004;24:10022-10034.
22. Türkyılmaz A, Tekin E, Yaralı O, Çebi AH. Genetic landscape of *SCN1A* variants in a Turkish cohort with GEFS+ spectrum and Dravet syndrome. *Mol Syndromol*. 2022;13:270-281.
23. Richards S, Aziz N, Bale S, et al. Standards and guidelines for the interpretation of sequence variants: a joint consensus recommendation of the American College of Medical Genetics and Genomics and the Association for Molecular Pathology. *Genet Med*. 2015;17:405-423.
24. Lomize MA, Pogozheva ID, Joo H, Mosberg HI, Lomize AL. OPM database and PPM web server: resources for positioning of proteins in membranes. *Nucleic Acids Res*. 2012;40:D370-D376.
25. Gabelli SB, Boto A, Kuhns VH, et al. Regulation of the $Na_V1.5$ cytoplasmic domain by calmodulin. *Nat Commun*. 2014;5:5126.
26. Waterhouse A, Bertoni M, Bienert S, et al. SWISS-MODEL: homology modelling of protein structures and complexes. *Nucleic Acids Res*. 2018;46:W296-W303.
27. Pettersen EF, Goddard TD, Huang CC, et al. UCSF Chimera—a visualization system for exploratory research and analysis. *J Comput Chem*. 2004;25:1605-1612.
28. Newport TD, Sansom MSP, Stansfeld PJ. The MemProtMD database: a resource for membrane-embedded protein structures and their lipid interactions. *Nucleic Acids Res*. 2019;47:D390-D397.
29. Floden EW, Tommaso PD, Chatzou M, Magis C, Notredame C, Chang JM. PSI/TM-coffee: a web server for fast and accurate multiple sequence alignments of regular and transmembrane proteins using homology extension on reduced databases. *Nucleic Acids Res*. 2016;44:W339-W343.
30. Robert X, Gouet P. Deciphering key features in protein structures with the new ENDscript server. *Nucleic Acids Res*. 2014;42:W320-W324.
31. Wu X, Hong L. Calmodulin interactions with voltage-gated sodium channels. *Int J Mol Sci*. 2021;22:9798.
32. Pires DEV, Rodrigues CHM, Ascher DB. mCSM-membrane: predicting the effects of mutations on transmembrane proteins. *Nucleic Acids Res*. 2020;48:W147-W153.
33. Moehring J, von Spiczak S, Moeller F, et al. Variability of EEG-fMRI findings in patients with *SCN1A*-positive Dravet syndrome. *Epilepsia*. 2013;54:918-926.
34. Gardill BR, Rivera-Acevedo RE, Tung CC, Okon M, McIntosh LP, van Petegem F. The voltage-gated sodium channel EF-hands form an interaction with the III-IV linker that is disturbed by disease-causing mutations. *Sci Rep*. 2018;8:4483.
35. Clairfeuille T, Cloake A, Infield DT, et al. Structural basis of α-scorpion toxin action on Na_v channels. *Science*. 2019;363:eaav8573.
36. Liu CJ, Dib-Hajj SD, Renganathan M, Cummins TR, Waxman SG. Modulation of the cardiac sodium channel $Na_v1.5$ by fibroblast growth factor homologous factor 1B. *J Biol Chem*. 2003;278:1029-1036.
37. Goetz R, Dover K, Laezza F, et al. Crystal structure of a fibroblast growth factor homologous factor (FHF) defines a conserved surface on FHFs for binding and modulation of voltage-gated sodium channels. *J Biol Chem*. 2009;284:17883-17896.
38. Ishikawa T, Kimoto H, Mishima H, et al. Functionally validated SCN5A variants allow interpretation of pathogenicity and prediction of lethal events in Brugada syndrome. *Eur Heart J*. 2021;42:2854-2863.
39. Li J, Yu Z, Xu J, et al. The effect of Ca^{2+}, lobe-specificity, and CaMKII on CaM binding to $Na_V1.1$. *Int J Mol Sci*. 2018;19:2495.
40. Lee A, Goldin AL. Role of the terminal domains in sodium channel localization. *Channels*. 2009;3:171-180.
41. Sharkey LM, Cheng X, Drews V, et al. The *ataxia3* mutation in the N-terminal cytoplasmic domain of sodium channel $Na_v1.6$ disrupts intracellular trafficking. *J Neurosci*. 2009;29:2733-2741.
42. Wang Z, Vermij SH, Sottas V, et al. Calmodulin binds to the N-terminal domain of the cardiac sodium channel $Na_v1.5$. *Channels*. 2020;14:268-286.
43. Wang J, Yarov-Yarovoy V, Kahn R, et al. Mapping the receptor site for alpha-scorpion toxins on a Na^+ channel voltage sensor. *Proc Natl Acad Sci*. 2011;108:15426-15431.
44. Osteen JD, Herzig V, Gilchrist J, et al. Selective spider toxins reveal a role for the $Na_v1.1$ channel in mechanical pain. *Nature*. 2016;534:494-499.

45. Wingerd JS, Mozar CA, Ussing CA, et al. The tarantula toxin β/δ-TRTX-Pre1a highlights the importance of the S1-S2 voltage-sensor region for sodium channel subtype selectivity. *Sci Rep*. 2017;7:974.
46. Jiang D, Tonggu L, Gamal El-Din TM, et al. Structural basis for voltage-sensor trapping of the cardiac sodium channel by a deathstalker scorpion toxin. *Nat Commun*. 2021;12:128.
47. Marco Hernández AV, Tomás Vila M, Caro Llopis A, Monfort S, Martinez F. Case report: novel homozygous likely pathogenic *SCN1A* variant with autosomal recessive inheritance and review of the literature. *Front Neurol*. 2021;12:784892.
48. Lindy AS, Stosser MB, Butler E, et al. Diagnostic outcomes for genetic testing of 70 genes in 8565 patients with epilepsy and neurodevelopmental disorders. *Epilepsia*. 2018;59:1062-1071.
49. Kapplinger JD, Tester DJ, Alders M, et al. An international compendium of mutations in the *SCN5A*-encoded cardiac sodium channel in patients referred for Brugada syndrome genetic testing. *Heart Rhythm*. 2010;7:33-46.
50. Smits JP, Eckardt L, Probst V, et al. Genotype-phenotype relationship in Brugada syndrome: electrocardiographic features differentiate *SCN5A*-related patients from non-*SCN5A*-related patients. *J Am Coll Cardiol*. 2002;40:350-356.
51. Smits JP, Koopmann TT, Wilders R, et al. A mutation in the human cardiac sodium channel (E161K) contributes to sick sinus syndrome, conduction disease and Brugada syndrome in two families. *J Mol Cell Cardiol*. 2005;38:969-981.
52. Xu X, Zhang Y, Sun H, et al. Early clinical features and diagnosis of Dravet syndrome in 138 Chinese patients with *SCN1A* mutations. *Brain Dev*. 2014;36:676-681.
53. Till Á, Zima J, Fekete A, et al. Mutation spectrum of the *SCN1A* gene in a Hungarian population with epilepsy. *Seizure*. 2020;74:8-13.
54. Fujiwara T, Sugawara T, Mazaki-Miyazaki E, et al. Mutations of sodium channel alpha subunit type 1 (*SCN1A*) in intractable childhood epilepsies with frequent generalized tonic-clonic seizures. *Brain*. 2003;126:531-546.

How to cite this article: Teralı K, Türkyılmaz A, Sağer SG, Çebi AH. Prediction of molecular phenotypes for novel *SCN1A* variants from a Turkish genetic epilepsy syndromes cohort and report of two new patients with recessive Dravet syndrome. *Clin Transl Sci*. 2024;17:e13679. doi:10.1111/cts.13679